Chinese Journal of
POLYMER SCIENCE

RESEARCH ARTICLE

https://doi.org/10.1007/s10118-024-3164-y
Chinese J. Polym. Sci. **2024**, *42*, 1780–1792

Conformational Disorder Within the Crystalline Region of Silica-Filled Polydimethylsiloxane: A Solid-State NMR Study

Yu-Qi Xiong[a,c], Chang-Lin Li[c], Ai Lu[c], Liang-Bin Li[a*], and Wei Chen[a,b*]

[a] *National Synchrotron Radiation Laboratory, Anhui Provincial Engineering Laboratory of Advanced Functional Polymer Film, CAS Key Laboratory of Soft Matter Chemistry, University of Science and Technology of China, Hefei 230026, China*
[b] *Department of Accelerator Science and Engineering Physics, School of Nuclear Science and Technology, University of Science and Technology of China, Hefei 230026, China*
[c] *Institute of Chemical Materials, China Academy of Engineering Physics, Mianyang 621900, China*

Electronic Supplementary Information

Abstract The crystallization behavior of silica-filled polydimethylsiloxane (PDMS) was investigated in detail by ^{1}H solid-state nuclear magnetic resonance (^{1}H SS-NMR) in combination with synchrotron radiation wide-angle X-ray scattering (WAXS), and temperature-modulated differential scanning calorimetry (TMDSC) techniques. For neat PDMS, no apparent difference is observed for the crystallinity characterized by ^{1}H SS-NMR and WAXS at low-temperature regions. However, upon filler addition, a 15%–35% lower difference in crystallinity is observed measured by ^{1}H SS-NMR compared to WAXS. The origin of such mismatch was explored through multi-component structural, dynamics, and chain-order analysis of PDMS samples with different filler fractions. The 1D integrated WAXS results of PDMS with different filler fractions at different temperatures show that the packing structure as well as crystal size basically remain unchanged, but as the filler fraction increases from 0 phr to 60 phr, the rigid component's dynamics order parameter S_r obtained by ^{1}H SS-NMR decreases from 0.70 to 0.55. The filler fraction-dependent crystallinity calculated based on S_r was compared with experimental values, revealing a behavior of decreasing order in the crystalline region. Combining with the results of accelerated chain dynamics in crystalline region as reflected by T_2 values, the molecular origin is attributed to the formation of CONDIS crystals, whose conformational order is lost but the position and orientation orders are kept. Such hypothesis is further supported by the TMDSC results, where, as the filler fraction increases from 0 phr to 60 phr, the melting range widens from 8.77 K to 14.56 K, representing a growth of 166%. In addition to previous reports related to the condition for forming CONDIS mesophase, *i.e.*, temperature, pressure, and stretching, the nano-sized filler could also introduce the local conformational disorder for chain packing.

Keywords Solid state NMR; Polymer nanocomposite; CONDIS crystal; Local chain order; PDMS crystallization

Citation: Xiong, Y. Q.; Li, C. L.; Lu, A.; Li, L. B.; Chen, W. Conformational disorder within the crystalline region of silica-filled polydimethylsiloxane: a solid-state NMR study. *Chinese J. Polym. Sci.* **2024**, *42*, 1780–1792.

INTRODUCTION

In contemporary academic and industrial realms, polydimethylsiloxane (PDMS) has garnered significant interest owing to its outstanding properties and diverse applications.[1–3] Notably, as one of the rare elastomers boasting exceptional resistance to low temperatures, PDMS exhibits unique utility in cryogenic environments.[4–6] It finds specific applications as sealing gaskets in low-temperature storage containers, as seals in cryogenic reactors, and as casings for low-temperature sensors, underscoring its unparalleled value in these specialized contexts.[5–7] However, PDMS tends to crystallize rapidly below its melting temperature (T_m≈228 K), leading to a significant decrease in its elasticity.[8,9] Under low-temperature stretching, PDMS exhibits polymorphic transitions and mesophases. The crystal structure of PDMS was proposed to be monoclinic with the 2_1-helix conformation (α-crystal) by Damaschun in 1962 after analyzing X-ray scattering patterns of filled PDMS samples (φ=35%) under large strains (λ=4).[10] Nonetheless, such molecular conformation is later challenged. The singlet NMR resonance lines of ^{13}C and ^{29}Si obtained by Schilling *et al.*[11] for unstretched pure PDMS contradicted such 2_1-helix structure, as a singlet NMR resonance line implied that all monomers were equivalent within the unit cell. Based on this, Albouy restudied the PDMS crystal structure under small strains in 2000,[12] proposing the tetragonal system with 4_1-helix structure (β-crystal) that was in line with the ^{13}C/^{29}Si-NMR results. However, such crystal structure requires further investigation as "the addition of some disorder appears necessary to account for the experimental line intensities".[12]

In addition to crystal structure determination, the phase

* Corresponding authors, E-mail: lbli@ustc.edu.cn (L.B.L.)
E-mail: wc003@ustc.edu.cn (W.C.)

Received April 7, 2024; Accepted May 14, 2024; Published online August 20, 2024

transition of PDMS under deformation attracts great attention as it is closely related to the macroscopic performance of PDMS under low-temperature regions. Tosaka *et al*.[13,14] characterized the stretch-induced crystallization process of PDMS using X-ray methods, indicating the stretching-induced phase transition between two crystals, namely, α- and β-crystal, and proposing a mesophase appearing during crystallization between them. To validate the non-equilibrium nature of the stretch-induced structural transition, Zhao *et al*.[8,9,15] constructed a non-equilibrium phase diagram in the strain-temperature space using a low-temperature *in situ* stretching method coupled with synchrotron radiation X-ray scattering, highlighting the effective manner in which phase transitions between crystal forms accommodate molecular strains and release strain energy during stretching. In their work, they noted that this mesophase exhibited a parallel helical structure similar to columnar phases, resembling the liquid crystal phase of polydiethylsiloxane (PDES).[16–18]

However, as of present, the investigation into the polycrystalline behavior of PDMS under low-temperature conditions remains insufficient, with a prevalent belief that liquid crystalline properties are absent in static samples.[19,20] In contrast, the crystal-to-crystal transitions and liquid crystalline regions of PDES have been extensively examined using various techniques, demonstrating the existence of "conformationally disordered crystals (CONDIS crystals)" within a temperature range of approximately 200–280 K.[19] One contributing factor is that the mesophase of PDMS has thus far only been detected under specific strains, and the 2θ values of the diffraction peaks of its α, β, and mesophase overlap, making the differences between the diffraction patterns of the crystal types observable solely from the intensity distribution of the azimuths after stretching.[9,15] Although Rabolt *et al*.[19] observed distinguishable bimodal melting peaks in the DSC data of low-molecular-weight PDMS, suggesting the potential existence of polycrystalline behavior, they have not provided a definitive explanation.

Furthermore, despite considerable research efforts in recent years focusing on understanding the crystallization behavior of PDMS, deliberate incorporation of fillers is imperative in many practical applications of silicon-based elastomeric materials to enhance their strength.[21,22] This becomes particularly crucial as pure silicone rubber exhibits significantly poor mechanical properties compared to other rubber materials. Hence, this complexity surpasses the challenges posed solely by investigating PDMS crystallization behavior. Typically, within the nanometer to tens of nanometers range on filler particle surfaces, significant changes occur in the structure, dynamics, interaction strength, thermal transitions, and properties of the polymer.[23–27] Besides the tightly bound layer (BL) formed by chemical crosslinking between polymer and particle surfaces, there also exists a loosely structured intermediate layer composed of adsorbed chains and locally restricted chains. These two components possess distinctly different physical or chemical properties and together constitute what is commonly referred to as the "interface".[27–29] Additionally, upon exceeding a certain percolation threshold, the formation of a three-dimensional network between fillers increases system complexity.[30,31] Such locally constrained structures may lead to redistribution of local stress and strain on PDMS chains, potentially resulting in crystalline destabilization behavior akin to that induced by stretching. However, systematic studies on how silica nanoparticle fillers influence the polymorphism of PDMS at low-temperature have yet to be conducted. Such research, characterizing the conformation, crystal structure, and dynamics upon which PDMS crystallization behavior relies, will provide a general understanding of methods to control its macroscopic wide-temperature performance.

In probing the molecular-level dynamics of intricate multi-component structures within composite materials, solid-state nuclear magnetic resonance (SS-NMR) presents substantial advantages.[32–37] By examining parameters such as transverse relaxation times T_2, relative fraction f, and local dynamics order parameter S as functions of composition or temperature variations, a wealth of information can be garnered.[38,39] SS-NMR provides insights into dynamics conformational disorder (exceeding the glass transition temperature, T_g), while at lower timescales, it enables the evaluation of methyl groups' rotational vibrations.[40] In the case of PDMS filled with silica, NMR methodologies have also been utilized to ascertain the extensive relaxation distribution of rubber chains adsorbed onto filler surfaces.[24,27,41–43]

In this study, we present a novel approach by combining ^{1}H SS-NMR with synchrotron radiation wide-angle X-ray scattering (WAXS) as well as the temperature-modulated differential scanning calorimetry (TMDSC) to investigate the crystallization behavior of PDMS filled with 0/10/40/60 phr silica in detail. Firstly, it was observed that the ^{1}H SS-NMR results below the melting temperature can decouple three components including the crystalline region through dynamics differences. Secondly, characterization of crystallinity at the same temperature and experimental conditions as ^{1}H SS-NMR was performed *via* synchrotron radiation WAXS, revealing significant discrepancies in crystalline fraction between the two techniques upon the introduction of fillers. An underestimation of crystallinity is observed for ^{1}H SS-NMR results. Analysis of the multi-component structure, dynamics, and local ordering evolution of PDMS samples with varying filler fractions suggests that heterogeneity in filler surface structure and consequent chain rearrangement induce a decrease in the stability of crystalline region ordering. This leads to a transition towards the mesophase, categorized as conformationally disordered (CONDIS) crystals exhibiting long-range positional and orientation order between the chain segments, yet disorder in chain conformation. This experiment delineates for the first time the polycrystalline behavior of PDMS in the unstretched state. Finally, the conclusions were further confirmed by TMDSC results.

EXPERIMENTAL

Samples

Polysiloxane composites investigated in this work were prepared using PDMS (VMQ, vinyl content=0.51%, ρ=1.1–1.2 g/cm^3, Chongqing Ruiya Biotechnology Co., Ltd.) reinforced with 0/10/40/60 phr fumed silica, respectively (The primary particle size of 15 nm and aggregate into clusters of about 200 nm in ethanol, ρ=2.2 g/cm^3, Technical Institute of Physics and

https://doi.org/10.1007/s10118-024-3164-y

Chemistry, CAS). Both the raw rubber was deliberately purchased with an ultra-high molecular weight of 650 kg/mol. Benzoyl peroxide (BPO, AR) as a vulcanizing agent was purchased from Shanghai Merrill Chemical Technology Co., Ltd.

Nanocomposite samples were mixed and sulfur vulcanized following general procedures. First, the raw rubber was added into an internal mixer under 60 r/min and 378 K for 5 min. The SiO_2 were then added to the polymer mix in three batches every 5 min until phase separation was no longer observed after blending. Whereafter, the mixture was taken out and re-melted for 15 minutes. The prepared mixture was placed for an additional 72 h at 298 K and 1.5 phr BPO was added using an open roll mill to avoid an early cross-linking reaction. The uncured rubber film was vulcanized in a 1 mm thick plate mold under pressure at 388 K for 30 min. The detailed chemical structure, ingredients, and preparation parameters are shown in Table 1 and Scheme S1 (in the electronic supplementary information, ESI). The VMQs with 0, 10, 40, 60 phr silica are denoted as VMQ0, VMQ10, VMQ40, VMQ60 (the corresponding volume fraction φ_f=0 vol%, 4.35 vol%, 15.38 vol%, 21.43 vol%), respectively. A nominal melting temperature of T_m=228 K for PDMS was determined as the peak in the DSC (second heating curve with a constant rate of 10 K/min, Fig. S1 in ESI) and the crystallization temperature for PDMS has been reported below 190 K.[44] Scanning electron microscope (SEM) was performed on a ZEISS GeminiSEM 500 operated at 3.00 kV on samples at room temperature. The SEM images with uniformly dispersed fillers can be seen in Fig. S2 (in ESI).

^{1}H SS-NMR Spectroscopy

^{1}H SS-NMR measurements were carried out on a mq20 Bruker minispecs with a ^{1}H Larmor frequency of 19.95 MHz. The π/2 and π pulses length was 2.85 and 5.60 μs, respectively. For variable-temperature (VT) tests, the samples were tested from 169 K to 333 K ($T_g \approx$ 158 K, as found in Fig. S3 in ESI) with the BVT 3000 working with liquid nitrogen. Prior to each measurement under a given temperature, the sample was pre-stabilized for 10 min. The recycle delay time of around 3 s. The 1 mm thick rubber films were cut up and placed into 8 mm diameter flat-bottom tubes. The sample height was limited to 10 mm to reduce the error caused by the magnetic field inhomogeneity. All VT experiments were conducted in the static state.

^{1}H Magic Sandwich Echo free induction decay (^{1}H MSE-FID) pulse sequence was used to refocus the signal loss during the dead time (14 μs) of the low-field NMR before ^{1}H SS-NMR signal acquisition.[45] The phase switching time (t_φ) was set as 0.002 ms while the number of cycles (n_{MSE}) was 1. For chopped rubber samples, 64 scans were adopted. The gain was identical for each sample during the VT-NMR experiments.

The attenuation of the transverse relaxation spectrum observed above the glass transition temperature (T_g) originates from a solid-like behavior induced by pure residual ^{1}H-^{1}H dipolar interactions. ^{1}H SS-NMR, which monitors dynamics by detecting changes in proton dipolar coupling interactions, reveals that the observed local anisotropic property primarily arises from the positional and orientational fluctuations of inter-nuclear vectors between adjacent proton pairs. Although interactions between protons in different bonds contribute to a minor relaxation mechanism, their impact is typically considered negligible at temperatures well above T_g.[24] For spin pairs with static dipolar coupling, the transverse relaxation function is defined as the average overall dynamics configurations of the bond angle $\theta(\tau)$.[46] At temperature well above T_g, the internal motion resulting from these complex effects can be described by a single correlation relaxation time, τ_c, based on the Anderson-Weiss (AW) theory.[47] Additionally, the local orientation dependence of molecular residues relative to the principal axis direction is commonly represented by a dynamics order parameter S,[48] which incorporates a second-order Legendre polynomial P_2:

$$\frac{I(t,T)}{I_0} = \left\langle \cos\left\{\int_{t'}^{t+t'} \omega[\theta(\tau)]\,d\tau\right\}\right\rangle = \exp\left\{\left(-\frac{1}{2}S^2M_2t^2\right) - \left(1-S^2\right)M_2\tau_c^2(T) \times \left[\exp\left(-\frac{t}{\tau_c(T)}\right) + \frac{t}{\tau_c(T)} - 1\right]\right\} \quad (1)$$

where $I(t,T)$ represents the decay of the NMR signal intensity with time t, due to the relaxation of excited protons at the test temperature T. I_0 represents the NMR signal intensity at t=0. M_2 is the second moment of the dipolar-broadened spectrum, which is a measure of the average static low-temperature limit dipole-dipole coupling in the system. For the fitting of NMR curves under given temperature, in order to obtain reasonable results, τ_c was assigned with boundary conditions consistent with the detection scale of the current NMR apparatus (ns–ms). Besides, all other parameters (S, M_2) were free parameters in the fitting.

WAXS Measurements

All WAXS measurements were conducted in the beamline 10U in Shanghai Synchrotron Radiation Facility. The incident X-ray wavelength is λ=0.124 nm. Two-dimensional (2D) WAXS diffraction patterns were collected using a Pilatus 900K detector. For temperature-dependent experiments, a Linkam thermal stage coupled with liquid nitrogen gas flow was employed. In the present work, the temperature range within the sample chamber was maintained between 183–213 K. Upon reaching the desired temperature during testing, the sample was stabilized for 10 min. Quantitative analysis was performed by converting 2D

Table 1 Sample recipe.

Sample	BPO [a] (phr [b])	SiO_2 (phr)	Volume fraction (vol%)
VMQ0	1.5	0	0
VMQ10	1.5	10	4.35
VMQ40	1.5	40	15.38
VMQ60	1.5	60	21.43

[a] Benzoyl peroxide; [b] Parts per hundred rubber by weight.

WAXD patterns into one-dimensional (1D) integrated intensity curves using the Fit2D software developed at the European Synchrotron Radiation Facility (ESRF).[49] Crystallinity ($\chi_{c,WAXS}$) is determined from the fitting results of multiple peaks in the 1D integrated WAXS curves. The fitted Gaussian peaks represent the crystalline and amorphous phases, respectively. The crystallinity (χ_c) is calculated using the equation:

$$\chi_c = \frac{\sum A_c}{\sum A_c + \sum A_{amor}} \times 100\% \quad (2)$$

where A_c and A_{amor} represent the areas under the crystalline and amorphous peaks in 1D integrated curves of WAXS curves, respectively, and the crystallinity of samples with varying filler fractions needs further correction based on PDMS mass fractions.

TMDSC Measurements

TMDSC of all samples was carried out on a TA Q2500. The VMQ/SiO_2 were first heated up to 150 ℃ and kept for 10 min to eliminate the thermal history, and then cooled down to 183 K with a cooling rate of 10 K/min. The TMDSC was carried out from 183 K to 313 K with a ramp rate of 2 K/min and modulation amplitude of ±1 ℃. The modulation period was set as 60 s.

RESULTS

VT NMR Measurement

^{1}H MSE-FID generates a well-focused decay for monitoring the dynamics of one or more components (n≥1) within the polymer, with the slow decay indicating the existence of a mobile polymer as well as the semi-rigid or rapid decay ^{1}H SS-NMR signals representing the presence of less mobile polymer contained in the initial fast decay part. The signal can be fitted using a combination of one or more modified Weibullian functions $\Sigma f_i \exp[-(t/T_{2,i})^{v_i}]$.[50] For rigid components such as the bound rubber or crystals, v_i=2; for the rubber matrix, v_i=1; while the semi-rigid interfacial layer with intermediate mobility falls between 1 and 2. The original VT ^{1}H MSE-FID curves of VMQ/SiO_2 samples have been arranged in Fig. S4 (in ESI), and an example of VMQ60 (225 K) original curves and corresponding fitting curves for n=1, 2, 3 are displayed in Fig. 1(a). The actual situation is even more intricate because, apart from the introduction of crystallization and fillers, which disrupt the dynamics uniformity of the system, temperature variations blur the distinctions between components and consequently influence the accuracy of the fitting. Bärenwald *et al.*[38] conducted an analysis by incorporating three-component fitting (including an Abragam component for rapid decay) to examine the relationship between the molecular weight and different forms of polyethylene (PE) with its crystallization behavior and local chain dynamics. Their perspective emphasizes the necessity of employing a three-component fitting approach to achieve satisfactory fitting quality. Papon *et al.*[45] validated the requirement for at least three components to accurately represent the temperature-dependent FID signals while investigating the influence of silica filler on the gradient dynamics heterogeneity of poly(ethyl acrylate) (PEA) materials. That is a fast mobility freely jointed chain below the melting temperature, a slow mobility constrained glassy polymer close to T_g, and an intermediate mobility layer. The latter two are obviously mixed with each other at low temperatures since FID is distinguished primarily by variations in component's dynamics. The reason for identifying three components in our study is that in the temperature range of T_g+30 K to T_g+70 K, there are clear differences where two components could not account for the observed behavior (see Fig. S5 in ESI). The relaxation time distribution of the semi-rigid domain starts to show distinct independence from the other two domains. Consequently, the form of the modified Weibullian function is determined as:

$$I_{norm}(t) = f_r \exp\left[-\left(\frac{t}{T_{2,r}}\right)^2\right] + f_{sr}\exp\left[-\left(\frac{t}{T_{2,sr}}\right)^{v_{sr}}\right] + f_m \exp\left[-\left(\frac{t}{T_{2,m}}\right)\right] \quad (3)$$

where r, sr and m stands for rigid, semi-rigid and mobile domains respectively with $f_r + f_{sr} + f_m = 1$; v_{sr} represents the shape factor of the NMR curve for the semi-rigid domain, taking values between 1 and 2; $T_{2,r}$, $T_{2,sr}$, $T_{2,m}$ respectively denote the transverse relaxation time of each domain. The fitting curves are shown in Fig. 1(b). Below T_m (228 K), the rigid domain in the VMQ/SiO_2 is comprised of at least two simultaneous constituents: crystalline region and BL (where the rigid domain of VMQ0 solely consists of crystalline region). The fitting results are shown in Figs. 1(c) and 1(d), it is evident that the rigid fractions ($f_{r,NMR}$) below T_m in VMQ/SiO_2 exceed 30%. A similar trend is also observed in the semi-rigid domain with $f_{sr,NMR}$≈60% at 180 K. Under the detection limit of the current device, it is challenging to distinguish between BL and the crystalline region in terms of dynamics. However, due to BL possessing a glass transition temperature significantly higher than that of the matrix,[51] structural damage will not occur in the current temperature range, resulting in a unchanged fraction. Therefore, constant BL fractions ($f_{bl,NMR}$) can be determined by the fraction of $f_{r,NMR}$ above T_m (Fig. S6 in ESI).

Synchrotron Radiation WAXS Measurements

In order to accurately quantify the crystalline fraction, the as-prepared VMQ/SiO_2 samples were employed for low-temperature (183–213 K) WAXS measurement. Fig. 2(a) presents the one-dimensional integrated WAXS curve of VMQ0 at 183 K which shows characteristic multiple Gaussian-fitted peaks corresponding to both crystalline and amorphous phases of PDMS below T_m. Meanwhile, the multi-peak deconvolution of the one-dimensional integrated WAXS curves was used to obtain crystallinity using Eq. (2) during the VT test, and the crystallinity was corrected based on the mass fraction of the polymer for samples with added fillers. Because ^{1}H SS-NMR only detects the proton signal from PDMS. The comparison between two different analytical techniques needs to remove the influence of the filler part. The temperature-dependent $\chi_{c,WAXS}$ is plotted in Fig. 2(b) (2D WAXS patterns and corresponding 1D curves can be found in Figs. S7 and S8 in ESI). Compared to the ^{1}H SS-NMR results, the low-temperature WAXS results reveal a higher overall crystallinity (30%–50%) at 183 K for the VMQ/SiO_2 samples. The details of the crystal structure in the VMQ/SiO_2 with different filler fractions can be elucidated through the full-widths at half maximum (FWHM) of various diffraction peaks β_{hkl} and 2θ obtained from the WAXS measurements, as shown in Figs. 2(c) and 2(d). It is observed that β_{hk} and 2θ remain constant across all systems, indicating that the influences related to filler-induced grain re-

finement behavior can be safely neglected. As mentioned in the introduction, distinguishment between stable crystalline and mesophase using WAXS poses a significant challenge, further analysis based on dynamics feature is necessary.

To facilitate a discussion under conditions approaching complete crystallization, the fitting results at two temperature points, 183 and 193 K, were selected for analysis. As illustrated in Fig. 3(a), the contrast in component fraction obtained through two distinct techniques highlights two key issues. Firstly, $\chi_{c,WAXS}$ unequivocally reveals an increase in crystallinity as the filler fraction rises. In contrast, the crystalline region (obtained by deducting $f_{bl,NMR}$ from $f_{r,NMR}$) is found to be the lowest in the VMQ60, which seems to present a conclusion markedly different from WAXS, indicating the filler suppresses crystallization. Another point worth mentioned is that the ^{1}H SS-NMR-measured VMQ60 exhibits the lowest $f_{r,NMR}$, while paradoxically exhibiting the highest $f_{sr,NMR}$. Generally speaking, within a specific polymer, be it as crystalline region or BL, the fraction of the semi-rigid domain forms between these structures and polymer correlates positively with the fractions of their components. In other words, the anomalous conclusion obtained through ^{1}H SS-NMR may stem from the fact that, unlike WAXS, which assesses the crystalline behavior of polymer materials based on long-range ordered, the ^{1}H SS-NMR method, relying on dynamics differences among different phases, may overlook the uncertainties related to the dynamics heterogeneity associated with the tightness of chain packing in the crystalline region. For instance, potential constraints or defects leading to partially disordered crystallites could manifest as relatively free chain mobility and disordered conformations.[52]

Taking into account the crystallinity variations highlighted in Fig. 3(a), it is hypothesized that parts of the crystalline region show relatively fast chain dynamics as compared with the remaining ones. From the aspect of chain dynamics by ^{1}H SS-NMR, they are categorized into semi-rigid domain. In this context, the crystalline portion accessed by the ^{1}H SS-NMR rigid component is defined as crystals ($f_{c,NMR}$), and the metastable phase possibly included in the semi-rigid domain is referred to as mesophases ($f_{me,NMR}$). The discrepancy between $\chi_{c,WAXS}$, and $f_{c,NMR}$ provides a straightforward quantification for $f_{me,NMR}$, as illustrated in Fig. 3(b). Such fraction significantly increases upon increasing filler fractions. As the filler fraction increases to 10 phr, $f_{me,NMR}$ rises from 1.98% to 18.55% (183 K). Subsequently, with a continuous increment in filler fraction up to 60 phr, $f_{me,NMR}$ further increases from

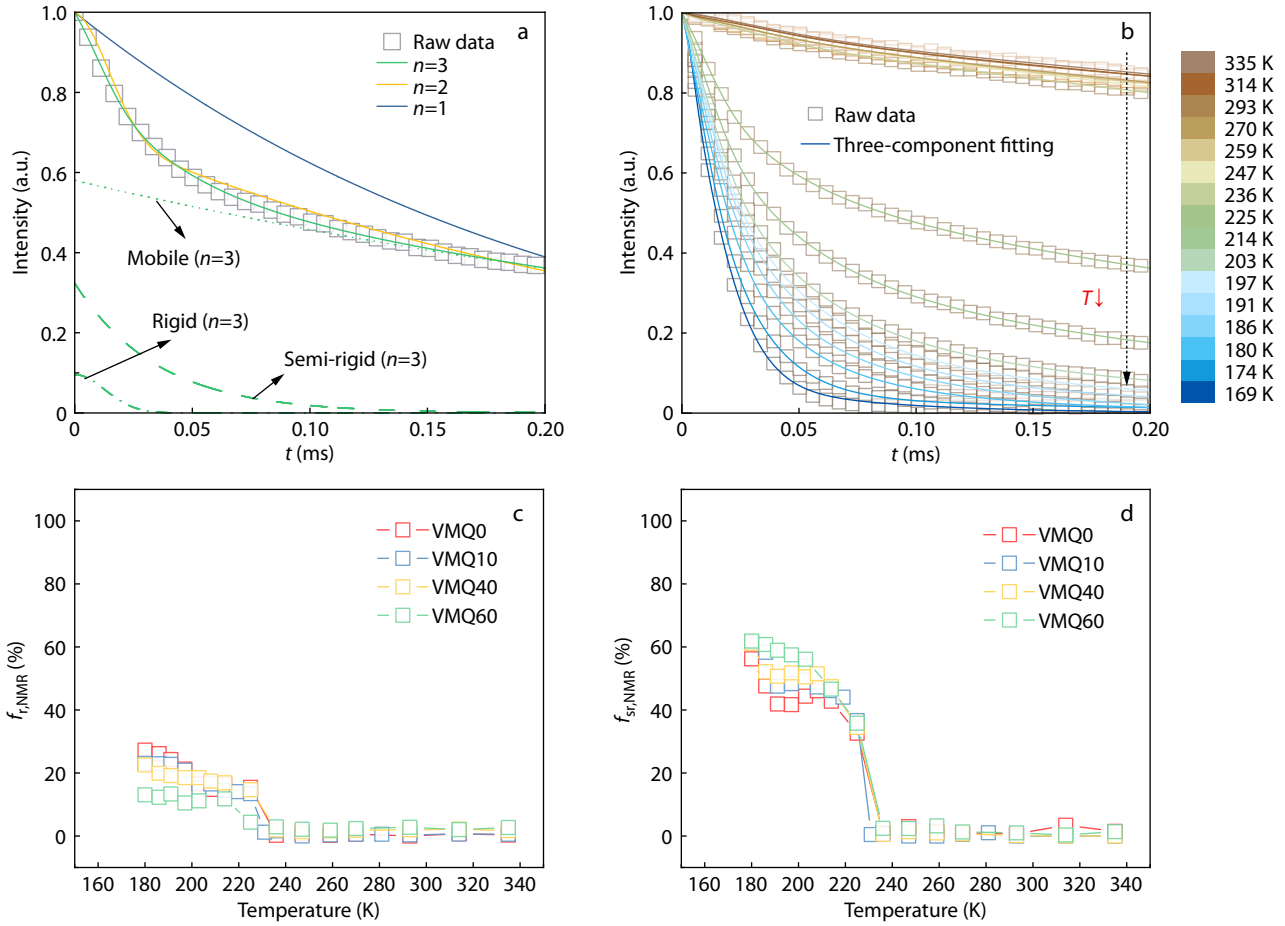

Fig. 1 (a) Typical one-component, two-component and three-component fitting (n=1, 2, 3) curves for the VMQ60 sample at 225 K and corresponding deconvolution curves of three-component fitting; (b) ^{1}H MSE-FID NMR signals for the VMQ60 at 169–335 K fitted with three-component fitting and fraction evolution of (c) rigid domain composed of bound layer and crystalline region and (d) semi-rigid domain of VMQ/SiO_2 samples as a function of experimental temperature.

https://doi.org/10.1007/s10118-024-3164-y

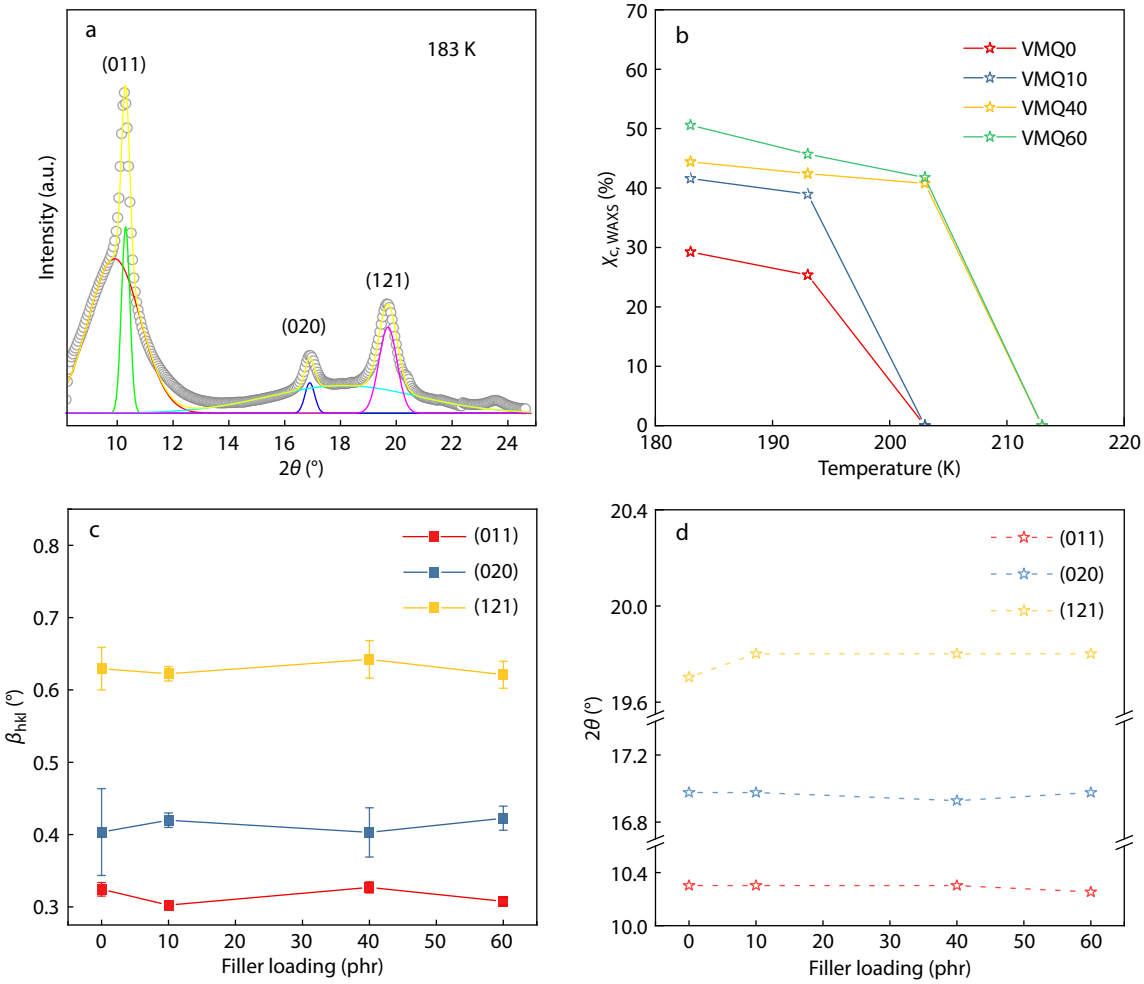

Fig. 2 (a) Illustration of multiple Gaussian peaks fit on the 1D integrated WAXS curve of crystallized PDMS; (b) Temperature dependent of crystallinity of VMQ/SiO_2; (c) Evolution of β_{hkl} (FWHM of various diffraction peaks) and (d) 2θ as a function of filler loading at 183 and 193 K.

18.55% to 36.21% (183 K). In order to elucidate potential factors associated with the filler, the theoretical $f_{me,NMR}$ at φ=0 vol% is obtained at the intercept of the filler fraction dependent $f_{me,NMR}$ to be approximately 13% (blue line), while $f_{me,NMR}$=1.98% at φ=0 vol% in actual ^{1}H SS-NMR measurement. It is important to note that such a difference represents an extreme scenario, indicating that if fillers are solely considered as high modulus additives without accounting for their interactions, the theoretically expected outcomes should demonstrate a positive correlation with filler fraction, particularly at lower filler fractions.[53] These findings imply that the increase in the fraction of mesophase does not stem from perturbations of the simple hydrodynamics of polymers induced by fillers.

Chain Dynamics Within PDMS Crystalline Region

In this section, ^{1}H SS-NMR was employed to monitor the effect of increasing filler fraction on the chain dynamics and local ordering of the rigid and semi-rigid components, respectively. The ^{1}H SS-NMR curves of these two components can be analyzed separately after deconvolution by Eq. (3). From the perspective of ^{1}H SS-NMR analysis, the chain dynamics within the highly ordered crystals in rigid domain result in an incomplete averaging of proton dipolar couplings, leading to a rapid decay of T_2. This decay can be accurately described by the Abragam equation with a sinusoidal function form, $\exp[-0.5(at)^2]\sin(bt)/(bt)$.[38] The second moment M_2 (calculated by $M_2 = a^2 + 1/3b^2$) of the Fourier transform of ^{1}H MSE-FID of strongly coupled spins can be utilized to quantify the extent of chain motion within the stable crystalline region. When the chain motion rate exceeds the ^{1}H-^{1}H dipolar coupling strength (about 20 kHz),[54] partial averaging of dipolar couplings occurs, leading to a decay in M_2. It should be noted that the AW equation (Eq. 1) can also be utilized for fitting M_2. However, the fitting results of M_2 and τ_c in this equation exhibit a certain correlation, necessitating the specification of the scale range of τ_c to obtain an accurate solution for M_2. In contrast, the Abragam equation offers higher accuracy and universality in obtaining M_2 for crystal components, the fitting schematic figure of NMR curves for rigid domain at different temperatures are illustrated in Fig. 4(a). Here, M_2 is employed to assess the chain segment dynamics of the stable crystalline region in rigid domain, and $T_{2,sr}$ obtained through Eq. (3) is utilized to evaluate the chain segment dynamics of semi-rigid domain.

For the characterization of local ordering, under the condition of a single principal axis, the local anisotropy within a specific region of the sample can be characterized by the or-

https://doi.org/10.1007/s10118-024-3164-y

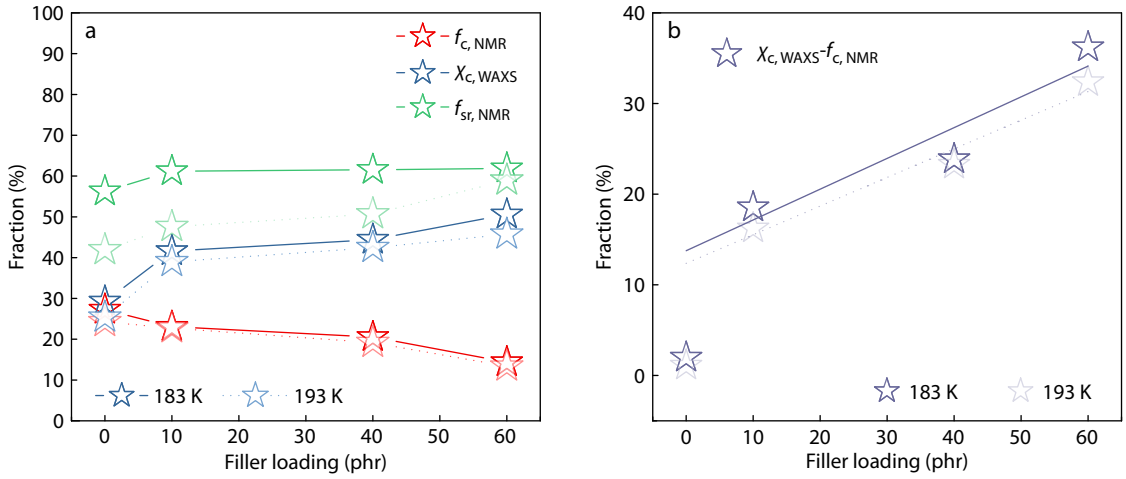

Fig. 3 (a) The comparison of the crystallinity obtained from WAXS ($\chi_{c,WAXS}$) and ^{1}H SS-NMR ($f_{c,NMR}$) experiments for PDMS with different silica filling fractions, and fraction evolution of semi-rigid domain ($f_{sr,NMR}$) for VMQ/SiO_2 samples at 183/193 K; (b) Evolution of $f_{me,NMR}$ (calculated by $\chi_{c,WAXS} - f_{c,NMR}$) for VMQ/$SiO_2$ samples as a function of filler loadings.

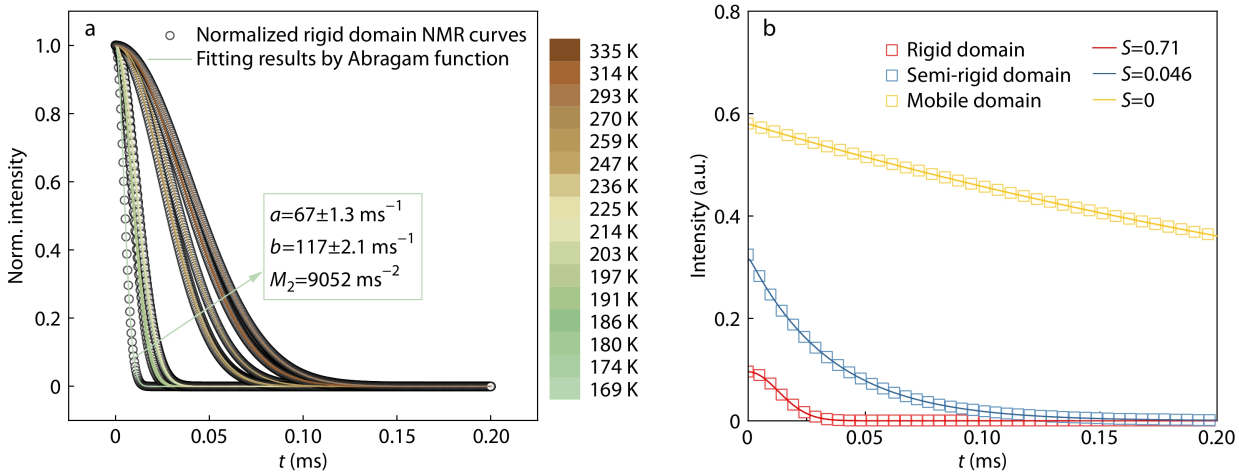

Fig. 4 (a) Illustrative example of fitting NMR curves for rigid domains at various temperatures using the Abragam equation. The figure depicts the fitting result of parameters a and b at 169 K, along with the calculated result for M_2; (b) Exemplary fitting based on the Anderson-Weiss function (Eq. 1) and decomposition of NMR data into its individual contribution. S is the order parameter, which is set to 0 for the isotropic mobile domain, and between 0 and 1 for the locally anisotropic rigid domain and intermediate domain.

der parameter S. The essence of this theory lies in defining the optimal orientation vector $\boldsymbol{n}$ within the region. In this defined region, all residual dipoles exhibit anisotropic directions that deviate to varying degrees from $\boldsymbol{n}$ and then S is utilized to quantify the degree of local order deviation. This concept has found extensive application in characterizing crystal structure.[55,56] For example, according to $P_2(\cos\theta)$, S=1 when the chain remains in the static state (rigid limit), and equals 0 when the chain exhibits isotropic rotation (mobile limit). Therefore, it serves as a useful order parameter to quantify molecular geometry. In this work, the order parameter S of each component is obtained by fitting the deconvoluted ^{1}H SS-NMR curves using Eq. (1), as seen in Fig. 4(b).

Chain dynamics and local ordering in the rigid domain

Fig. 5(a) illustrates the obtained M_2 and its temperature dependence for all VMQ/SiO_2 samples. As mentioned above, M_2 indicates the proton dipolar coupling strength in the crystalline region. A slight decay in M_2 is observed from 169 K to 228 K, which is attributed to the thermal-activated lattice expansion.[36] Furthermore, there was no difference in the M_2 values of samples with varying filler fractions, indicating that the presence of filler has no effect on the chain dynamics in the crystalline region at this time scale. On the contrary, Fig. 5(b) presents detailed information on the fluctuations in order parameter S within the rigid domain of the VMQ/SiO_2 composites. The results reveal a decrease in S from 0.70 to 0.55 as the filler fraction increases from 0 phr to 60 phr. The origin of the decreasing S can be attributed to two main factors: one is the decrease in the relative fraction of stable crystals in the rigid component, and the other is the intrinsic decreasing order of the stable crystals. These speculations were substantiated by comparing the theoretically calculated proportion of stable crystals in the rigid component $f_{c,NMR}/f_{r,NMR}$, obtained through order parameters, with the actual proportion, as illustrated in Fig. 5(c). The ensemble order parameter S obtained through Eq. (1), allows for a correlation of the contributions of these two rigid components.

https://doi.org/10.1007/s10118-024-3164-y

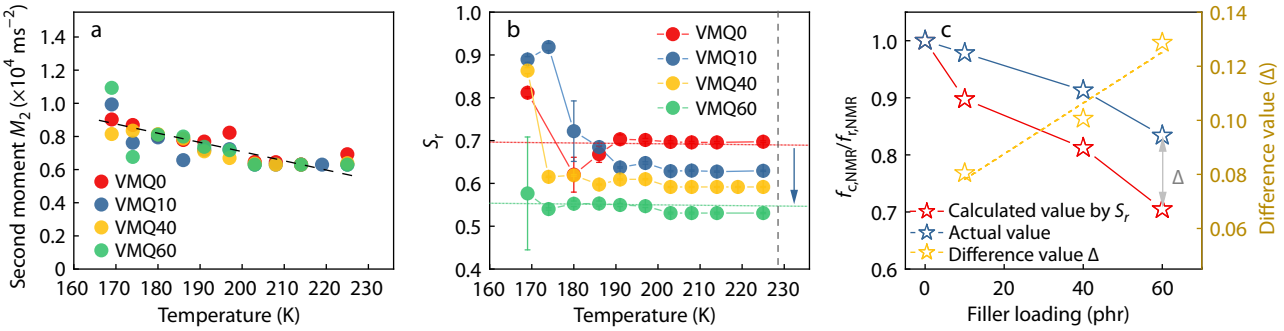

Fig. 5 (a) Temperature dependence of the second moment M_2 calculated from the Abragam function; (b) Effect of rigid confinements on local order and segmental dynamics as observed by ^{1}H SS-NMR. Data are given as a function of experimental temperature. (c) Theoretical $f_{c,NMR}/f_{r,NMR}$ values obtained through Eq. (4) for VMQ/SiO_2 samples compared with experimental data for validation. Δ corresponds to the difference value between the two.

$$S = f_{bl,NMR}S_{bl,NMR} + f_{c,NMR}S_{c,NMR} \quad (4)$$

$$f_{r,NMR} = f_{c,NMR} + f_{bl,NMR} \quad (5)$$

where the constants S_{bl} and S_c are set at 0.13 and 0.70, respectively (S_{bl} was obtained *via* rigid components of non-crystalline systems with similar conditions, as shown in Fig. S9 in ESI). In the observed results, the red stars represent the proportion of theoretical $f_{c,NMR}/f_{r,NMR}$ calculated by Eq. (4), and the portion lower than 1 solely represents a relative decrease in the stable crystal fraction attributed to the increasing filler fraction. The blue stars represent experimental $f_{c,NMR}/f_{r,NMR}$ values. Evidently, beyond a filler loading of 10 phr, there is approximately a 10% deviation between the theoretical and experimental values. This indicates that increasing filler fraction results in decreasing stable crystal fraction and local order parameter. The latter, relative to filler fraction, can be quantified by the difference value Δ between theoretical and experimental values, as illustrated by the yellow stars in Fig. 5(c). As the filler fraction increases from 10 phr to 60 phr, Δ increases from 0.08 to 0.13. Orientation disorder also represents a pathway of crystal disorder. However, pure orientation disorder does not directly lead to faster chain dynamics, and WAXS results did not reveal any changes in chain packing. Therefore, combining the results of WAXS and ^{1}H SS-NMR, such disorder is consistent with the classification of conformational disorder (CONDIS). In this study, the molecular origin for the presence of the conformation disorder is proposed to be related to the filler as discussed in the following section.

Chain dynamics and local ordering in the semi-rigid domain

For polymer chains attached to rigid components, including interfacial chains extending from the bound layer and interphase chains connected to the stable crystal, all fall within the semi-rigid domain. Due to the considerably more complex mathematical relationships of multicomponent systems, achieving detailed decoupling in analysis is challenging, thus permitting only a reasonable qualitative analysis. In Fig. 6(a), $T_{2,sr}$ of semi-rigid domain obtained *via* ^{1}H SS-NMR are depicted as a function of temperature. Within this temperature range, there is no significant difference in dynamics among the samples with different filler additions. Conversely, with increasing filler fraction, there is a marked increase in the order parameter S_{sr} (Fig. 6b). Indeed, the local ordering of the semi-rigid domain is greatly influenced by the ordering of the rigid components to which they are attached, and the same applies to the amorphous regions. Thus, throughout the interface from the filler surface to away from the filler, these characteristic values exhibit a gradient-like decay. If only considering the segments connected to the bound layer and crystal in the semi-rigid domain, which inherit the crystalline ordering completely, the S_{sr} of the VMQ0 is theoretically the highest. However, the actual observation results are contrary, indicating the presence of structures with higher local ordering. Here, we consider such decreasing order parameter to be contributed from the mesophases. Fig. 6(c) illustrates the S_{sr} values as a function of the relative fraction of mesophases in semi-rigid domain. The pronounced linear relationship therein attests to the correlation between the two. This observation further corroborates the hypothesis that fillers lead to relatively fast chain dynamics in crystalline region.

Temperature Modulated DSC

As a typical method for characterizing polycrystalline materials,

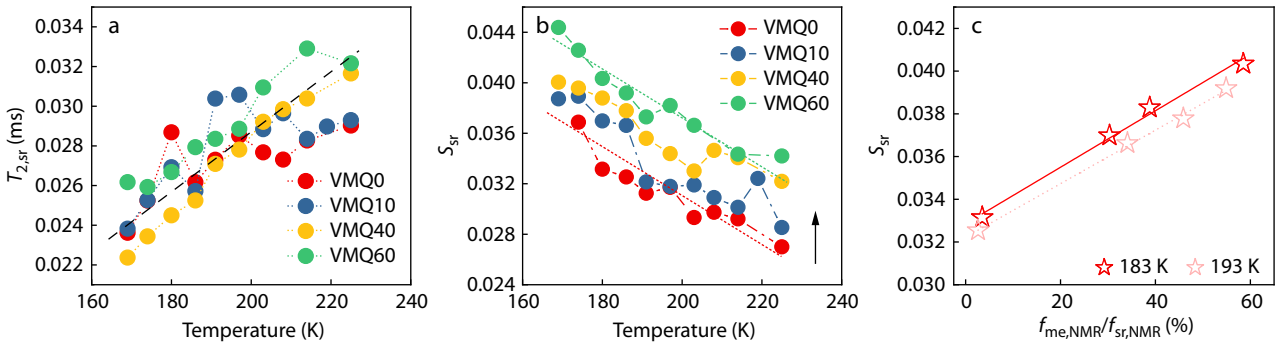

Fig. 6 Evolution of (a) $T_{2,sr}$ and (b) S_{sr} for VMQ/SiO_2 samples as a function of experimental temperatures; (c) S_{sr} values as a function of the relative fraction of mesophases in semi-rigid domain $f_{me,NMR}/f_{sr,NMR}$.

https://doi.org/10.1007/s10118-024-3164-y

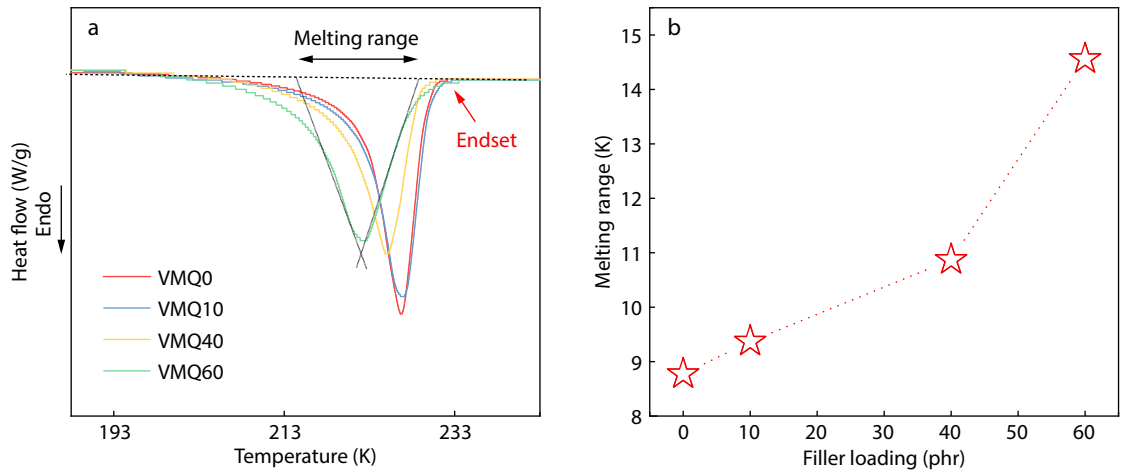

Fig. 7 (a) TMDSC thermograms after peak height normalization of VMQ/SiO_2 samples with modulate temperature amplitude of ±1 K and modulation period of 60 s; (b) Evolution of melting range as a function of filler loadings.

our conclusions were cautiously validated through TMDSC analysis. Fig. 7(a) depicts the TMDSC curves of VMQ/SiO_2. These samples were cooled from the melt state to 183 K before measurements and held isothermally for ten minutes. Upon melting of these crystals, endothermic peaks can be observed around 223 K. Noticeable differences among samples with different filler fractions were observed in their respective melting temperatures and melting ranges. With increasing filler fraction, the melting temperature gradually decreased, indicating a decrease in the stability of crystals. More importantly, the increasing melting range (Fig. 7b) confirms the existence of CONDIS crystals, as this behavior, in the absence of significant changes in crystal structure and size, is attributed to molecules or atoms undergoing various conformational states during the melting process.[52]

DISCUSSION

Through the combination of ^{1}H SS-NMR, WAXS and TMDSC measurements, three key findings are summarized as follows. (1) Increasing crystallinity difference obtained by ^{1}H SS-NMR and WAXS, respectively, with increasing filler fraction (Fig. 3), whereas invisible change is observed for 1D integrated WAXS curves (Fig. S8 in ESI); (2) decreasing segmental order parameter *S* in the crystalline region with increasing filler fraction by ^{1}H SS-NMR (Fig. 5c); (3) increasing melting range with increasing silica filling fraction by TMDSC (from 8.77 K for VMQ0 to 14.56 K for VMQ60, showing a growth of 166%, Fig. 7b). Such results suggest the presence of the CONDIS crystal in PDMS crystalline region. Note, this holds for silica-filled PDMS but fails for pure PDMS systems (Fig. 3). Detailed descriptions for above hypothesis of the presence of CONDIS crystal are presented in the following section.

Enhanced Chain Dynamics in the Crystalline Region

The underestimated crystallinity by ^{1}H SS-NMR is attributed to the enhanced chain dynamics in the crystalline region, where partial of the protons are assigned to the semi-rigid component (Fig. 3b). Direct evidence comes from the decreasing dynamics order parameter *S* with increasing filler fraction (Fig. 5b). In addition to dynamics information, the structure information as shown by the 1D integrated WAXS curve shows no visible difference in peak position and FWHM is almost the same for different samples at different temperatures (Figs. 2c and 2d). In spite of polymorphism in PDMS, *i.e.*, α, β and mesophases, their 1D integrated WAXS curves are identical where apparent difference is observed in 2D WAXS patterns.[15] Two possible reasons could be responsible for the above results: one is the presence of CONDIS crystal, and the other is the α_c relaxation in the crystalline region, both of which show enhanced chain dynamics in the crystalline region without structure change. The thermal activated α_c relaxation can be excluded based on the following considerations. The α_c relaxation refers to the segmental relaxation in the crystalline region at temperatures well above the glass transition temperature T_g but below the melting temperature T_m.[57] For the α_c relaxation, segments take helical-jump or π-flip motion within the crystalline region,[39,58] whose dynamics order parameter *S* is inversely proportional to the available jump sites *N*.[38,59] Considering the continuous decrement of *S* upon filler addition, the dynamics feature of the α_c relaxation is different from the above results of PDMS. Additionally, no report related to the existence of the α_c relaxation for PDMS has been found. This is consistent with temperature-dependent M_2 (Fig. 5a), where only a slight decay is observed. Such decrement is attributed to the thermal-activated lattice expansion as mentioned above.[38] As a result, the presence of CONDIS crystal is proposed to explain the origin of the enhanced chain dynamics in the crystalline region. For CONDIS crystal, the position and orientation orders are kept, whereas the molecular conformation order is lost, resulting in a metastable phase as compared with stable crystal. The continuous decreasing *S* could be attributed to increasing CONDIS crystal fraction upon filler addition.

Thermal Behavior

Thermal transitions involved in the process of crystalline transition or polycrystalline behavior are typically measured by TM-DSC. The TM-DSC is frequently used to investigate the presence of mesophase as well as the phase transition from mesophase to crystal.[19,60–62] For semicrystalline polymer, the melting temperature of the mesophase, or CONDIS crystal in the

current study, is normally lower than that of stable crystal. Therefore, phenomena such as the presence of multiple independent melting peaks or broadened peaks can be used as evidence for the presence of mesophase in combination with other analytical characterization techniques. For instance, after annealing, additional melting peaks corresponding to the growth of small-sized mesophases were observed in the *i*PP, and their peak size increased with the annealing temperature.[60] PDES, on the other hand, was found to exist in both monoclinic and tetragonal forms within the range of 203–213 K, and undergo a transition to a liquid crystal phase around 278–288 K.[19] In the current work, the TMDSC results provide evidence for the above hypothesis of the introduction of CONDIS crystal in the presence of filler. The crystallization temperature T_c increases with increasing filler addition (Fig. 2b), whereas the corresponding melting temperature T_m decreases continuously (Fig. 7). Such a result suggests decreasing nucleation barrier and crystal stability in the presence of filler. Additionally, the melting range increases from 8.77 K (0 phr) to 14.56 K (60 phr). These are well consistent with the above hypothesis where more CONDIS crystals are introduced upon increasing filler fraction.

Critical Role of Filler

Above conclusion agrees with early Wunderlich's work on pure PDMS, where he regarded PDMS as a model polymer without mesophase complexity.[20] For another silicone rubber, poly(diethyl siloxane) (PDES), the CONDIS crystal exists for the filler-free sample at a low-temperature region (*ca.* 206.7 K).[20] Compared with PDMS, PDES owns longer flexible side chains. The interactions between ethyl side groups and backbone chain are believed to influence the helix to coil transition at the molecular level, leading to the loss of order in PDES during the melting process from the disordered crystalline region to the isotropic liquid phase, while also affecting its conformation and translational mobility.[63] From the aspect of the chemical structure feature, semicrystalline polymer with flexible side chains can form CONDIS crystals, *i.e.*, isotactic poly(1-butene) (*i*PB1) and PDES, where the high chain dynamics of these side chains can stabilize these phases.[64–67] For polymers without such flexible side chains, *i.e.*, polyethylene (PE), the CONDIS crystal exists under high pressure or deformation conditions,[68,69] because crystallization under such conditions inevitably leads to higher mobility of chains within the crystal, thereby generating extended-chain crystals from the initially grown chains folded into macroscopic configurations.[70] For silica-filled PDMS, the CONDIS mesophase is previously observed under deformation conditions at low-temperature regions,[15] whereas the presence of CONDIS crystal under quiescent conditions has rarely been reported. Different from the CONDIS crystal in other semicrystalline polymers, for silica-filled PDMS, such phase coexists with the more stable crystal (Fig. 8). Compared with the stable crystal, the CONDIS crystal keeps the position and orientation orders but loses the conformational order, and their coexistence complicates the structural analysis of silica-filled PDMS. Generally, the CONDIS crystal, or mesophase,[52] can be formed by following conditions: (1) temperature, which is the most reported parameter, *i.e.*, PDES, *i*PP;[19,70] (2) pressure, *i.e.*, PE,[68,69] polytetrafluoroethylene (PTFE);[71] (3) stretching, *i.e.*, PDMS,[14] PE.[72] In the current study, our results suggest the introduction of nano-sized filler can also lead to the appearance of such a phase. The introduction of the filler significantly influences the chain dynamics in the crystalline region: the higher filler fraction, the higher the component fraction of the faster chain dynamics in the crystalline region. Cohen *et al.*[73] conducted a similar study examining the impact of fillers on PDMS crystallization. They proposed that the topological constraints induced by fillers would impede the orderly growth of crystallization. Such disorder is originally proposed by Albouy as "the addition of some disorder appears necessary to account for the experimental line intensities", which is in line with current work.[12] Additionally, recent work by Lotz in addressing the rigid amorphous fraction (RAF) suggests "the RAF is actually a 'condis oriented' fraction".[74] This shows for the chain packing structure in the interface, such conformation disorder widely exists. Chains in the crystalline region of the filled PDMS cooled from the melt state experience an unbalanced conformational distribution due to the local constraints of interfacial dynamics heterogeneity, leading to a partial transformation towards CONDIS crystals. Overall, the mobility of these chains significantly increases, yet the average long-range order of PDMS crystals remains unchanged, resulting in discrepancies between the characterization results of WAXS and ^{1}H SS-NMR, as illustrated in Fig. 8.

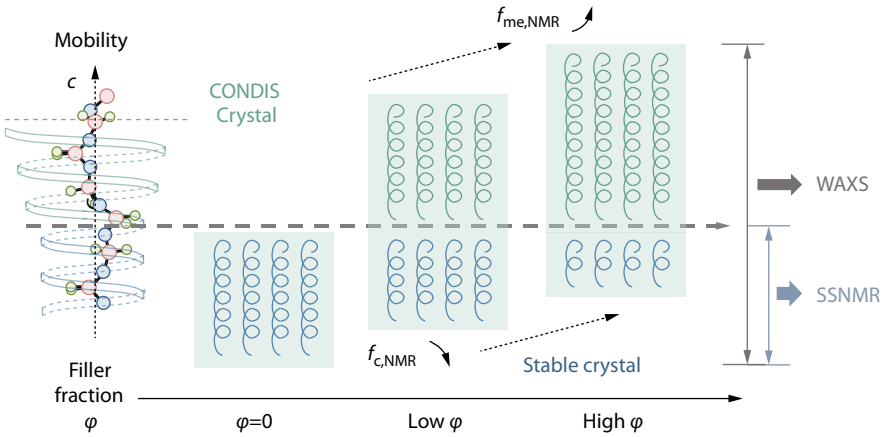

Fig. 8 Diagram illustrating the conformational disorder of PDMS induced by filler.

https://doi.org/10.1007/s10118-024-3164-y

CONCLUSIONS

The present work investigated the influence of fillers on the crystallization behavior of PDMS through ^{1}H SS-NMR combined with WAXS and TMDSC techniques, demonstrating that the introduction of fillers leads to the formation of a crystal structure with positional and orientational order but conformational disorder. This molecular origin is attributed to the formation of CONDIS crystals, combined with the faster chain dynamics reflected in the ^{1}H SS-NMR results. Three key experimental results support such hypothesis: (1) for filled PDMS samples, ^{1}H SS-NMR shows a 15-35% lower crystallinity compared to WAXS, but no difference is observed in pure samples; (2) as the filler fraction increases, the local order parameter of stable crystals decreases; (3) the melting range of the samples increases from 8.77 K to 14.56 K with filler fraction increases from 0 phr to 60 phr. These experimental results provide key evidence for the coexistence of polymorphism and the ordered-disordered transition in PDMS under static conditions. Previously, such behavior had only been studied in diffraction patterns of stretched samples. This is because PDMS exhibits an anomalous feature where the diffraction angle remains nearly constant during the crystalline region transition, only manifesting differences in the integrated intensity distribution of azimuthal angles after stretching. Furthermore, in addition to previous reports related to the formation of CONDIS mesophase under conditions of temperature, pressure, and stretching, the evidence from this study suggests that nano-sized fillers may also introduce local conformational disorder for chain packing.

Lastly, it is worth emphasizing that our current tools do not provide a comprehensive understanding of all the intricacies of the multilevel structure in composite materials. Investigation related to the spatial proximity of the CONDIS crystal and stable crystal is still required. Nevertheless, in terms of observing local segmental order, SS-NMR exhibits clear advantages, particularly when applied to rescaled single chains and constrained network chains. In the investigation of PDMS crystallization behavior, dynamics order parameters offer direct evidence of the extent of segmental ordering, facilitating a thorough exploration of the underlying mechanisms by which filler particles influence the crystallization behavior. Furthermore, it is important to note that dynamics order parameters undeniably present a novel approach for characterizing the dynamics of locally constrained network chains within the intermediate polymer domain at the molecular level.

Conflict of Interests

Liang-Bin Li is an editorial board member for *Chinese Journal of Polymer Science* and was not involved in the editorial review or the decision to publish this article. All authors declare that there are no competing interests.

Electronic Supplementary Information

Electronic supplementary information (ESI) is available free of charge in the online version of this article at http://doi.org/10.1007/s10118-024-3164-y.

ACKNOWLEDGMENTS

This work was financially supported by NSAF Joint Fund of China (No. U2030203), the National Natural Science Foundation of China (Nos. 51973207 and 51903230) and the experimental assistance from Shanghai Synchrotron Radiation Facility (SSRF) for WAXS measurement are greatly appreciated.

REFERENCES

1 Nguyen, D. T.; Meyers, C.; Yee, T. D.; Dudukovic, N. A.; Destino, J. F.; Zhu, C.; Duoss, E. B.; Baumann, T. F.; Suratwala, T.; Smay, J. E.; Dylla-Spears, R. 3D-printed transparent glass. *Adv. Mater.* **2017**, *29*, 1701181.
2 Choi, S.; Lee, H.; Ghaffari, R.; Hyeon, T.; Kim, D. H. Recent advances in flexible and stretchable bio-electronic devices integrated with nanomaterials. *Adv. Mater.* **2016**, *28*, 4203–4218.
3 Beigbeder, A.; Linares, M.; Devalckenaere, M.; Degée, P.; Claes, M.; Beljonne, D.; Lazzaroni, R.; Dubois, P. CH-π interactions as the driving force for silicone-based nanocomposites with exceptional properties. *Adv. Mater.* **2008**, *20*, 1003–1007.
4 Zhang, G.; Sun, Y.; Qian, B.; Gao, H.; Zuo, D. Experimental study on mechanical performance of polydimethylsiloxane (PDMS) at various temperatures. *Polym. Test.* **2020**, *90*, 106670.
5 Niu, S.; Chang, X.; Zhu, Z.; Qin, Z.; Li, J.; Jiang, Y.; Wang, D.; Yang, C.; Gao, Y.; Sun, S. Low-temperature wearable strain sensor based on a silver nanowires/graphene composite with a near-zero temperature coefficient of resistance. *ACS Appl. Mater. Interfaces* **2021**, *13*, 55307–55318.
6 Xu, X.; Li, X.; Liu, G.; Wei, X.; Feng, D.; Zhang, L. Rational design of high-flux, eco-friendly, and versatile superhydrophobic/superoleophilic PDMS@ZIF-7/$Cu_3(PO_4)_2$ mesh with self-cleaning property for oil-water mixture and emulsion separation. *Inorg. Chem.* **2023**, *62*, 3260–3270.
7 Arkles, B. Look what you can make out of silicones. *Chemtech* **1983**, *13*, 542–555.
8 Zhao, J.; Feng, S.; Zhang, W.; Chen, W.; Sheng, J.; Yu, W.; Li, L. Strain rate dependence of stretch-induced crystallization and crystal transition of poly(dimethylsiloxane). *Macromolecules* **2021**, *54*, 9204–9216.
9 Zhao, J.; Chen, P.; Lin, Y.; Chen, W.; Lu, A.; Meng, L.; Wang, D.; Li, L. Stretch-induced intermediate structures and crystallization of poly(dimethylsiloxane): the effect of filler content. *Macromolecules* **2020**, *53*, 719–730.
10 Damaschun, G. Röntgenographische Untersuchung der Struktur von Silikongummi. *Kolloid-Zeitschrift Zeitschrift für Polym.* **1962**, *180*, 65–67.
11 Schilling, F.C.; Gomez, M.A.; Tonelli, A.E. Solid-state NMR observations of the crystalline conformation of poly(dimethylsiloxane). *Macromolecules* **1991**, *24*, 6552–6553.
12 Albouy, P.A. The conformation of poly(dimethylsiloxane) in the crystalline state. *Polymer* **2000**, *41*, 3083–3086.
13 Tosaka, M.; Noda, M.; Ito, K.; Senoo, K.; Aoyama, K.; Ohta, N. Strain- and temperature-induced polymorphism of poly(dimethylsiloxane). *Colloid Polym. Sci.* **2013**, *291*, 2719–2724.
14 Tosaka, M.; Tashiro, K. Crystal polymorphism and structure models of poly(dimethylsiloxane). *Polymer* **2018**, *153*, 507–520.
15 Zhao, J.; Chen, P.; Lin, Y.; Chang, J.; Lu, A.; Chen, W.; Meng, L.; Wang, D.; Li, L. Stretch-induced crystallization and phase transitions of poly(dimethylsiloxane) at low temperatures: an *in situ* synchrotron radiation wide-angle X-ray scattering study. Macromolecules **2018**, *51*, 8424–8434.
16 Hedden, R. C.; Tachibana, H.; Duncan, T. M.; Cohen, C. Effects of molecular structure on segment orientation in poly(diethylsiloxane) elastomers. 2. NMR measurements from

uniaxially stretched samples. *Macromolecules* **2001**, *34*, 5540–5546.
17 Batra, A.; Hedden, R. C.; Schofield, P.; Barnes, A.; Cohen, C.; Duncan, T. M. Conformational behavior of guest chains in uniaxially stretched poly(diethylsiloxane) elastomers: ^{2}H NMR and SANS. *Macromolecules* **2003**, *36*, 9458–9466.
18 Hedden, R. C.; Tachibana, H.; Duncan, T. M.; Cohen, C. Effects of molecular structure on segment orientation in siloxane elastomers. 1. NMR measurements from compressed samples ronald. *Macromolecules* **2001**, *34*, 3285–3293.
19 Friedrich, J.; Rabolt, J. F. Structural studies of phase transitions in poly(di-*n*-alkylsiloxanes). 1. Poly(dimethylsiloxane) and poly(diethylsiloxane). *Macromolecules* **1987**, *20*, 1975–1979.
20 Varma-Nair, M.; Wesson, J. P.; Wunderlich, B. The thermal properties of polysiloxanes poly(dimethyl siloxane) and poly(diethyl siloxane). *J. Therm. Anal.* **1989**, *35*, 1913–1939.
21 Kumar, S. K.; Benicewicz, B. C.; Vaia, R. A.; Winey, K. I. 50th Anniversary perspective: are polymer nanocomposites practical for applications? *Macromolecules* **2017**, *50*, 714–731.
22 Pérez-Aparicio, R.; Vieyres, A.; Albouy, P. A.; Sanséau, O.; Vanel, L.; Long, D. R.; Sotta, P. Reinforcement in natural rubber elastomer nanocomposites: breakdown of entropic elasticity. *Macromolecules* **2013**, *46*, 8964–8972.
23 Litvinov, V. M.; Steeman, P. A. M. EPDM-carbon black interactions and the reinforcement mechanisms, as studied by low-resolution ^{1}H NMR. *Macromolecules* **1999**, *32*, 8476–8490.
24 Fernández-De-Alba, C.; Jimenez, A. M.; Abbasi, M.; Kumar, S.K.; Saalwächter, K.; Baeza, G. P. On the immobilized polymer fraction in attractive nanocomposites: T_g gradient versus interfacial layer. *Macromolecules* **2021**, *54*, 10289–10299.
25 Cui, W.; You, W.; Sun, Z.; Yu, W. Decoupled polymer dynamics in weakly attractive poly(methyl methacrylate)/silica nanocomposites. *Macromolecules* **2021**, *54*, 5484–5497.
26 Salatto, D.; Carrillo, J. M. Y.; Endoh, M. K.; Taniguchi, T.; Yavitt, B. M.; Masui, T.; Kishimoto, H.; Tyagi, M.; Ribbe, A. E.; Garcia Sakai, V.; Kruteva, M.; Sumpter, B. G.; Farago, B.; Richter, D.; Nagao, M.; Koga, T. Structural and dynamical roles of bound polymer chains in rubber reinforcement. *Macromolecules* **2021**, *54*, 11032–11046.
27 Xiong, Y.; Xia, Z.; Lu, A.; Chen, W. Time-resolved extensional rheo-NMR spectroscopy for investigating polymer nanocomposites under deformation. *Anal. Chem.* **2023**, *95*, 7545–7551.
28 Hanakata, P. Z.; Douglas, J. F.; Starr, F. W. Interfacial mobility scale determines the scale of collective motion and relaxation rate in polymer films. *Nat. Commun.* **2014**, *5*, 1–8.
29 Popov, I.; Carroll, B.; Bocharova, V.; Genix, A. C.; Cheng, S.; Khamzin, A.; Kisliuk, A.; Sokolov, A. P. Strong reduction in amplitude of the interfacial segmental dynamics in polymer nanocomposites. *Macromolecules* **2020**, *53*, 4126–4135.
30 Chen, L.; Wu, L.; Song, L.; Xia, Z.; Lin, Y.; Chen, W.; Li, L. The recovery of nano-sized carbon black filler structure and its contribution to stress recovery in rubber nanocomposites. *Nanoscale* **2020**, *12*, 24527–24542.
31 Song, L.; Wang, Z.; Tang, X.; Chen, L.; Chen, P.; Yuan, Q.; Li, L. Visualizing the toughening mechanism of nanofiller with 3D X-ray nano-CT: stress-induced phase separation of silica nanofiller and silicone polymer double networks. *Macromolecules* **2017**, *50*, 7249–7257.
32 Besghini, D., Mauri, M., Roberto, S. Time Domain NMR in Polymer Science: From the Laboratory to the Industry. *Appl. Sci.* **2019**, *9*, 1801.
33 Saalwächter, K. Artifacts in transverse proton NMR relaxation studies of elastomers. *Macromolecules* **2005**, *38*, 1508–1512.
34 Maus, A.; Hertlein, C.; Saalwächter, K. A robust proton NMR method to investigate hard/soft ratios, crystallinity, and component mobility in polymers. *Macromol. Chem. Phys.* **2006**, *207*, 1150–1158.
35 Wu, Z.; Xiong, Y.; Li, C.; Cheng, H.; Li, Y.; Chen, W. Exploring the interphase structure of poly(vinyl alcohol) during sol-gel transition using selective probes with varied molecular sizes. *Macromolecules* **2023**, *56*, 7113–7124.
36 Jin, X.; Zhang, Q.; Xiong, Y.; Wu, Z.; Cheng, H.; Chen, X.; Chen, W. Molecular mechanism of surface melting of polyamide12 as elucidated by synchrotron radiation X-ray scattering and ^{1}H spin diffusion NMR. *Macromolecules* **2024**, *57*, 1227–1290.
37 Zhang, R.; Chen, W.; Miyoshi, T. Elucidations of structure and molecular dynamics of complex polymers by state-of-the-art solid-state NMR spectroscopy. *Macromolecules* **2024**.
38 Bärenwald, R.; Champouret, Y.; Saalwächter, K.; Schäler, K. Determination of chain flip rates in poly(ethylene) crystallites by solid-state low-field ^{1}H NMR for two different sample morphologies. *J. Phys. Chem. B* **2012**, *116*, 13089–13097.
39 Kurz, R.; Achilles, A.; Chen, W.; Schäfer, M.; Seidlitz, A.; Golitsyn, Y.; Kressler, J.; Paul, W.; Hempel, G.; Miyoshi, T.; Thurn-Albrecht, T.; Saalwächter, K. Intracrystalline jump motion in poly(ethylene oxide) lamellae of variable thickness: a comparison of NMR methods. *Macromolecules* **2017**, *50*, 3890–3902.
40 Schmidt-Rohr, K. Multidimensional Solid-State NMR and Polymer, Max-Planck-Institut für Polymerforschung, **2012**.
41 Litvinov, V. M.; Spiess, H. W. Molecular mobility in the adsorption layer and chain orientation in strained poly(dimethylsiloxane) networks by ^{2}H NMR. *Die Makromol. Chemie* **1992**, *193*, 1181–1194.
42 Litvinov, V. M.; Spiess, H. W. ^{2}H NMR study of molecular motions in polydimethylsiloxane and its mixtures with aerosils. *Die Makromol. Chemie* **1991**, *192*, 3005–3019.
43 Litvinov, V. M.; Spiess, H. W. ^{1}H and ^{2}H NMR study of chain motion at the poly(dimethylsiloxane)-filler interface. *Makromol. Chemie. Macromol. Symp.* **1991**, *44*, 33–36.
44 Aranguren, M. I. Crystallization of polydimethylsiloxane: effect of silica filler and curing. *Polymer* **1998**, *39*, 4897–4903.
45 Papon, A.; Saalwächter, K.; Schäler, K.; Guy, L.; Lequeux, F.; Montes, H. Low-field NMR investigations of nanocomposites: Polymer dynamics and network effects. *Macromolecules* **2011**, *44*, 913–922.
46 Brereton, M.G. NMR transverse relaxation function calculated for constrained polymer chains: application to entanglements and networks. *Macromolecules* **1990**, *23*, 1119–1131.
47 Anderson, P. W.; Weiss, P. R. Exchange narrowing in paramagnetic resonance. *Rev. Mod. Phys.* **1953**, *35*, 269–276.
48 Maier, V.W.; Saupe, A. Eine einfache molekulare Theorie des nematischen kristallinflüssigen Zustandes. *Naturforschg* **1958**, *13*, 564–566.
49 Hammersley A. ESRF97HA02T FIT2D: an introduction and overview. *J. Eur. Synchrotron Radiat. Facil. Intern. Rep.* **1997**, *68*, 58.
50 Weibull, W. A statistical distribution function of wide applicability. *J. Appl. Mech.* **1951**, *103*, 293–297.
51 Guy, L.; Saalwa, K. Glass-transition temperature gradient in nanocomposites : evidence from nuclear magnetic resonance and differential scanning calorimetry. *Phys. Rev. Lett.* **2012**, *108*, 065702.
52 Wunderlich, B. Thermodynamic description of condensed phases. *J. Therm. Anal. Calorim.* **2010**, *102*, 413–424.
53 Smallwood, H. M. Limiting law of the reinforcement of rubber. *J. Appl. Phys.* **1944**, *15*, 758–766.
54 Saalwächter, K.; Heuer, A. Chain dynamics in elastomers as investigated by proton multiple-quantum NMR. *Macromolecules* **2006**, *39*, 3291–3303.
55 Eslami, H.; Khanjari, N.; Müller-Plathe, F. A local order parameter-based method for simulation of free energy barriers in crystal

nucleation. *J. Chem. Theory Comput.* **2017**, *13*, 1307–1316.
56 Eslami, H.; Sedaghat, P.; Müller-Plathe, F. Local bond order parameters for accurate determination of crystal structures in two and three dimensions. *Phys. Chem. Chem. Phys.* **2018**, *20*, 27059–27068.
57 Hu, W. G.; Schmidt-Rohr, K. Polymer ultradrawability: the crucial role of a-relaxation chain mobility in the crystallites. *Acta Polym.* **1999**, *50*, 271–285.
58 Bärenwald, R.; Goerlitz, S.; Godehardt, R.; Osichow, A.; Tong, Q.; Krumova, M.; Mecking, S.; Saalwächter, K. Local flips and chain motion in polyethylene crystallites: a comparison of melt-crystallized samples, reactor powders, and nanocrystals. *Macromolecules* **2014**, *47*, 7677–7678.
59 Chen, W.; Reichert, D.; Miyoshi, T. Helical jump motions of poly(l-lactic acid) chains in the *α* phase as revealed by solid-state NMR. *J. Phys. Chem. B* **2015**, *119*, 4552–4563.
60 Androsch, R.; Lorenzo, M. L. Di; Schick, C.; Wunderlich, B. Mesophases in polyethylene, polypropylene, and poly(1-butene). *Polymer* **2010**, *51*, 4639–4662.
61 Wiedemann, H. G.; Wunderlich, B.; Wesson, J. P. Mesophase transition of polydiethylsiloxane. *Mol. Cryst. Liq. Cryst. Inc. Nonlinear Opt.* **1988**, *155*, 469–475.
62 Li, Z.; Miyoshi, T.; Sen, M.K.; Koga, T.; Otsubo, A. Solid-state NMR characterization of the chemical defects and physical disorders in *α* form of isotactic poly(propylene) synthesized by ziegler-natta catalysts. *Macromolecules* **2013**, *46*, 6507–6519.
63 Shibanov, Y. D. Optical properties of polydiethylsiloxane mesophase. *Polym. Sci. U.S.S.R.* **1989**, *31*, 2653–2662.
64 Wunderlich, B. Conformational motion and disorder in low and high molecular mass crystals. *Adv. Polym. Sci.* **1988**, *87*, 1.
65 Ungar, G. Thermotropic hexagonal phases in polymers: common features and classification. *Polymer* **1993**, *34*, 2050–2059.
66 Allegra, G.; Meille, S. V. Mesomorphic phases of flexible polymers: the self-compacting chain model. *Macromolecules* **2004**, *37*, 3487–3496.
67 Allegra, G. Interphases and Mesophases in Polymer Crystallization II. *Springer-Verlag Berlin Heidelberg*. **2005**, 153–177.
68 Bassett, D. C.; Block, S.; Piermarini, G. J. A high-pressure phase of polyethylene and chain-extended growth. *J. Appl. Phys.* **1974**, *45*, 4146–4150.
69 Yasuniwa, M.; Enoshita, R.; Takemura, T. X-ray studies of polyethylene under high pressure. *Jpn. J. Appl. Phys*. **1976**, *15*, 1421–1428.
70 Cocca, M.; Androsch, R.; Righetti, M. C.; Malinconico, M.; Lorenzo, M. L. Di. Conformationally disordered crystals and their influence on material properties: The cases of isotactic polypropylene, isotactic poly(1-butene), and poly(l-lactic acid). *J. Mol. Struct.* **2014**, *1078*, 114–132.
71 Starkweather, H. W. Comparison of the rheological properties of polytetrafluoroethylene below its melting point with certain low-molecular smectic states. *J. Polym. Sci., Polym. Phys. Ed.* **1979**, *17*, 73–79.
72 Wunderlich, B.; Grebowicz, J. Thermotropic mesophases and mesophase transitions of linear, flexible macromolecules. *Adv. Polym. Sci*. **1984**, 1–59.
73 Ebengou, R. H.; Cohen-Addad, J. P. Silica-poly(dimethylsiloxane) mixtures: n.m.r, approach to the crystallization of adsorbed chains. *Polymer* **1994**, *35*, 2962–2969.
74 Lotz, B. Fold surfaces of polymer crystals are nucleation sites: the link between polymer decoration, secondary crystallization, and the rigid amorphous fraction (RAF). *Macromolecules* **2023**, *56*, 4135–4152.